applied sciences

MDPI

Article

# Zeolite-Supported Ni Catalysts for $CO_2$ Methanation: Effect of Zeolite Structure and Si/Al Ratio

**Javier Francisco da Costa-Serra, Cristina Cerdá-Moreno and Antonio Chica ***

Instituto de Tecnología Química, Universitat Politècnica de València-Consejo Superior de Investigaciones Científicas, Avenida de los Naranjos s/n, 46022 Valencia, Spain; jdacosta@itq.upv.es (J.F.d.C.-S.); cricermo@itq.upv.es (C.C.-M.)

* Correspondence: achica@itq.upv.es

Received: 27 June 2020; Accepted: 23 July 2020; Published: 26 July 2020


**Abstract:** The urgent need to reduce $CO_2$ emissions requires the development of efficient catalysts for the conversion of $CO_2$ into chemicals and fuels. In this study, a series of nickel catalysts supported on ITQ-2 and ZSM-5 zeolites have been prepared, characterized and tested in the hydrogenation reaction of $CO_2$ towards methane. Specifically, two ITQ-2 and two ZSM 5 zeolites with different aluminum content have been studied. For both types, the higher Si/Al ratio of the material, the more active the catalyst due probably to its higher hydrophobicity. The largest difference was found for the ITQ-2 samples, being the $CO_2$ conversion for the sample with a greater Si/Al ratio 50 points higher at 350 °C. Comparing both zeolite structures, while similar catalytic results were obtained with the samples with lower Si/Al ratio, a distinctly higher activity was found for the ITQ-2 zeolite without aluminum, pure silica. Therefore, this result suggests that the presence of aluminum is of particular relevance. Among the studied materials, the catalyst supported on the delaminated ITQ-2 zeolite without Al was the most active catalyst. Its higher activity was mainly attributed to the smaller crystallite size of nickel supported on the large external surface area presented by this zeolite.

**Keywords:** $CO_2$ methanation; $CO_2$ hydrogenation; Ni-based catalysts; zeolites; delaminated zeolites; ITQ-2; Si/Al ratio

## 1. Introduction

Due to the growing concern about climate change and its consequences, most countries worldwide seem determined to take action against this problem. The relation of human-related activities with climate change is clear. Indeed, in the fifth assessment report of the Intergovernmental Panel on Climate Change (IPCC), these human activities are stated as the dominant cause with an extreme likelihood [1]. The impact of humankind on the climate system has been evidenced one more time during the outbreak and spread of COVID-19 disease in 2020. The confinement measurements adopted by most countries to slow down the expansion of this disease have produced a significant reduction of air pollution and $CO_2$ emissions due to the decline in human activity [2–4].

With the aim of unifying the response to mitigate climate change, the parties of the United Nations Framework Convention on Climate Change (UNFCCC) reached the Paris Agreement at the 21st session of the Conference of Parties (COP21) in December 2015. It is nowadays ratified by more than 180 countries and its main aim is to keep the global temperature rise below 2 °C above preindustrial levels [5]. In order to fulfill this aim, global net anthropogenic $CO_2$ emissions should decline by about 25% by 2030 and reach net zero around 2070. Therefore, the reduction of $CO_2$ emissions is urgently required [6].

Among the alternatives reported for the carbon capture, storage and utilization (CCSU), $CO_2$ hydrogenation appears as a feasible way to produce fuels and chemicals and, simultaneously, reduce

$CO_2$ anthropogenic emissions and storage renewable energy surplus. In particular, the hydrogenation of $CO_2$ towards methane has gained renewed interest recently. $CO_2$ methanation (also known as Sabatier reaction) is a highly exothermic reaction and although it is thermodynamically favorable [7,8], the use of a catalyst is needed to activate at low temperatures the stable molecule of $CO_2$ and selectively form methane.

In the last years, catalysts containing transition metals mainly of groups 8-11 of the periodic table (Ni, Ru, Rh, Co) have been found to be active for $CO_2$ methanation reaction [9–12]. Because of its high activity and selectivity as well as its comparatively low price, Ni-based catalysts are the most widely investigated materials. Generally, these active metals are widespread on another material to enlarge the active area of the catalyst. The material used as support not only plays a key role in the state of the active phase, but also usually influences itself the adsorption and catalytic properties of the catalyst.

Common supports for $CO_2$ methanation catalysts are oxides such as $Al_2O_3$, $CeO_2$, $ZrO_2$, $TiO_2$ or $SiO_2$, among others [9–12]. Preparation of highly dispersed and stable supported metal catalysts is generally one of the main aims. This can be achieved by the addition of promoters. For example, Lu et al. [13] found that the addition of $VO_x$ enhanced the catalytic properties of the material by the improvement in Ni dispersion. The use of $La_2O_3$ is also reported to enhance Ni reducibility and dispersion as well as the presence of moderate basic sites [14,15].

Another parameter influencing metal dispersion is the surface area of the support. For $CeO_2$, the catalytic activities increased with increasing surface area of $CeO_2$ [16]. For this reason, the use of supports with high surface area has also been considered. Aziz et al. [17] reported a Ni catalyst supported on mesostructured silica nanoparticles (MSN), which was found to be more active than other similar samples supported on MCM-41, HY, $SiO_2$ and $\gamma$-$Al_2O_3$.

Zeolites are another kind of potential material to prepare catalysts for $CO_2$ methanation. They offer, apart from a high surface area, good hydrothermal stability, flexible chemical composition and unique microporous structure. Even though their considerable versatility, few groups focused on them for $CO_2$ methanation reaction. Recently, Bacariza et al. [18] reviewed the studies on this field showing that parameters such as the preparation conditions [19–23], framework type [15,20,24], Si/Al ratio [24,25] or compensating cation [26] strongly affects the catalytic properties of the final material. The increase of calcination temperature is reported to favor the formation of sintered NiO nanoparticles in more internal locations of the zeolite. This migration of Ni species generally leads to a shift to higher temperature in TPR profiles [19,20]. Regarding reduction, the selection of a high temperature results in a greater amount of reduced Ni, but also produces nanoparticle sintering, reducing the active surface [19]. Another parameter affecting the size of the nanoparticles in zeolite is the metal precursor. Wei et al. [20] found that the use of citrate and acetate yields smaller NiO particle size in comparison with nitrate. Furthermore, the Ni loading [23], the method used to incorporate the elements of the catalyst [21–23] and the order of incorporation of these elements have been also studied [21,22].

Zeolites that are used as support for methanation catalysts are normally exchanged with sodium. Quindimil et al. [15] reported that the exchange of the protons by sodium in zeolites Y and Beta results in an enhancement of both Ni reducibility and weak $CO_2$ adsorption sites. However, in a previous study no influence on Ni reducibility was observed by the addition of different cations to ultrastable zeolite Y (USY) [26]. Also in this study, the following order was established for the enhancement of catalytic activity using Ni catalysts supported on cation exchanged zeolites: $Cs^+ > Na^+ > Li^+ > K^+ > H^+$ and $Mg^{2+} > Ca^{2+} > Ba^{2+}$ [26]. Independently of the compensating cation ($H^+$, $Na^+$, $Cs^+$), an improvement of the catalytic performance was achieved increasing the Si/Al ratio of USY zeolite [25]. This trend was against what was expected, attending to the basicity of the materials, as samples with high Al content (lower Si/Al ratio) present higher $CO_2$ adsorption capacity. However, it can be ascribed to the more hydrophobic character of the catalysts supported on zeolites of a higher Si/Al ratio [25].

By this time, different zeolite structures have been considered as supports for $CO_2$ methanation catalysts: USY [15,23], Beta [15,24], ZSM-5 [24], 13X [20] and 5A [20]. The type of zeolite used is reported to have an influence on the hydrophobicity of the final catalyst [24] as well as on the location

and reducibility of Ni nanoparticles [15,20]. As far as we know, the particular structure of delaminated zeolites has not been considered for $CO_2$ methanation reaction. This kind of material provides a very high external surface area, which increases the accessibility to the active sites maintaining the properties of the zeolite and making these materials a promising option to prepare highly dispersed metal catalysts.

Therefore, the aim of this work is to gain insight into the effect of the structure of the zeolite used as support and its Si/Al ratio on the catalytic performance for $CO_2$ methanation reaction. For this purpose, four zeolitic materials were used: two ITQ-2 and two ZSM-5, differing the zeolites of each type in the Al content, to prepare catalysts with 5 wt.% of Ni. These samples have been characterized and tested in $CO_2$ methanation reaction.

## 2. Materials and Methods

### 2.1. Catalyst Preparation

Ni catalysts were prepared by incipient wetness impregnation. First, the proper amount of the Ni precursor ($Ni(NO_3)_2{\cdot}6H_2O$) (Sigma-Aldrich, Madrid, Spain) was dissolved in water to achieve a 5 wt.% Ni in the final material. Then, this solution was added dropwise to the zeolite used as a support. In each case, the total volume of the solution was adjusted to the pore volume of the zeolite. After drying, the samples were calcined at 450 °C for 3 h.

Regarding the zeolite materials, ITQ-2 were synthesized starting from the corresponding zeolite precursors: ITQ-1 for pure silica ITQ-2 and MCM-22 for ITQ-2 with Si/Al ratio of 15. The synthesis of these precursors is described elsewhere [27]. The first step was the swelling of the precursor. Typically, 5 g of the precursor was dispersed in 100 g of an aqueous solution of hexadecyltrimethylammonium (CTMA) (Acros Organics, Madrid, Spain) bromide/hydroxide (40 wt.%, exchange of bromides by hydroxide of 50%) and 30 g of tetrapropylammonium (TPA) (Sigma-Aldrich, Madrid, Spain) bromide/hydroxide (25 wt.%, exchange of 30%) and the mixture was refluxed for 16 h at 52 and 80 °C for ITQ-2(∞) and ITQ-2(15), respectively. Then, the layers were forced apart by placing the slurry in an ultrasound bath (50 W, 40 kHz) for 1 h. After the ultrasound treatment, the solid was collected by acidification with concentrated hydrochloric acid (Fisher Scientific, Madrid Spain) until pH was below 2 and then by centrifuging. Finally, the organic material was removed by calcination at 540 °C, yielding ITQ-2.

Commercial ZSM-5, CBV3024E and CBV28014 (Zeolyst International, Delfzijl, Netherlands) with Si/Al ratios of 15 and 140, respectively, were used as starting materials. These two zeolites with ammonium as compensating cation were calcined at 500 °C for 3 h to obtain the acidic form.

The nomenclature of the catalysts used in this study is: xNi/YYY(z), where x is the Ni content, YYY the type of zeolite and z the Si/Al ratio.

### 2.2. Characterization

X-ray diffraction (XRD) patterns were recorded with a PANalytical CUBIX diffractometer (Philips, Amsterdam, The Netherlands) using Cu Kα radiation operating at 45 kV and 40 mA. The crystallite size for NiO was determined using the Scherrer equation.

Chemical composition (Ni, Si and Al content) of the materials was analyzed by inductively coupled plasma optical emission spectrometry (ICP-OES) on a Varian 715-ES (Agilent, Santa Clara, CA, USA).

Textural properties were determined from $N_2$ adsorption isotherms at −196 °C, recorded on a Micromeritics ASAP 2420 (Micromeritics Instrument Corporation, Norcross, GA, USA). Prior to the measurements, about 250 mg of the sample were outgassed under vacuum at 350 °C.

Temperature programmed reduction (TPR) was performed using a Micromeritics Autochem 2910 with a TCD detector (Micromeritics Instrument Corporation, Norcross, GA, USA). The sample (75 mg)

was first treated with Ar at room temperature for 15 min and then, in a flow of Ar and $H_2$ (50 mL/min, 10% of $H_2$), the temperature was raised up to 900 °C recording the $H_2$ consumption.

Brønsted acidity was evaluated by means of pyridine adsorption/desorption followed on a Nicolet 710 FTIR spectrometer (Thermo Scientific, Waltham, Massachusetts, USA). The sample (10−15 mg) was pressed to obtain a self-supported wafer, which was then pretreated at 400 °C in a vacuum overnight. After activation, pyridine vapor (650 Pa) was introduced to the cell at room temperature and desorbed at different temperatures (150, 250 and 350 °C). The spectrum of the sample after activation and after the desorption at each temperature was recorded at room temperature and the quantification of Brønsted sites was calculated according to Emeis [28].

Particle size distribution of reduced Ni ($Ni^0$) was determined by means of high-resolution transmission electron microscopy (HR-TEM) (JEM 2100F) (Akishima, Tokio City, Japan).

Carbon content was determined by elemental analysis (EA) on a EuroVector EuroEA (Eurovector, Pavia, PV, Italy).

### 2.3. Catalytic Activity

The catalytic activity for $CO_2$ methanation of these materials was evaluated in a fixed-bed reactor at atmospheric pressure, temperatures between 250 and 450 °C and 9000 mL/($g_{cat}$·h). In a typical experiment, 0.750 g of calcined catalyst (pellet size: 0.25−0.42 mm particle size) was diluted with silicon carbide (pellet size: 0.6−0.8 mm particle size) to achieve a volume of 5 $cm^3$. Prior to catalysis, the catalyst was reduced in situ passing through the reactor a flow of pure $H_2$ while the temperature was increased up to 450 °C and kept at this temperature for 2 h. After the reduction step, the temperature was lowered to the first reaction temperature, typically 250 °C, and then the reaction mixture (125 mL/min, $CO_2$:$H_2$:$N_2$ = 9:36:5) was fed into the reactor.

The outlet composition was analyzed on a Varian 3800 gas chromatograph (GC) (Agilent, Santa Clara, CA, USA). $CO_2$ conversion and $CH_4$ selectivity were calculated following (1) and (2), respectively, using $N_2$ as the internal standard.

$$X_{CO_2}(\%) = \frac{\dot{n}_{CO_2,\mathrm{i}} - \dot{n}_{CO_2,\mathrm{f}}}{\dot{n}_{CO_2,\mathrm{i}}} \times 100 \quad (1)$$

$$S_{CH_4}(\%) = \frac{\dot{n}_{CH_4,\mathrm{f}}}{\dot{n}_{CH_4,\mathrm{f}} + \dot{n}_{CO,\mathrm{f}}} \times 100 \quad (2)$$

where $\dot{n}_{CO_2}$, $\dot{n}_{CH_4}$ and $\dot{n}_{CO}$ are the molar flows of $CO_2$, $CH_4$ and CO, respectively, and the subscripts, i and f refer to the values at the input or output of the reactor.

## 3. Results and Discussion

### 3.1. Characterization

The XRD patterns of the zeolites used as support and the final catalysts after calcination are presented in Figure 1. These diffractograms confirm that the original structure of both zeolite types, ITQ-2 and ZSM-5, is preserved after Ni incorporation and calcination. For the sample supported on the ITQ-2 without Al, the absence of diffraction peaks of NiO indicates that Ni is well-dispersed in this sample with a small crystallite size (Figure 1a). The absence of diffraction peaks related to NiO for this catalyst indicates that the size of this phase might be probably under 3 nm, as the determination of crystallite sizes by XRD is reported to be applied more accurately in the range between 3 and 100 nm [29]. For the ITQ-2 zeolite with a Si/Al ratio of 15, the peaks corresponding to the NiO phase can be observed. The calculation of the crystallite size for NiO by Scherrer equation gives a result of 10.6 nm.

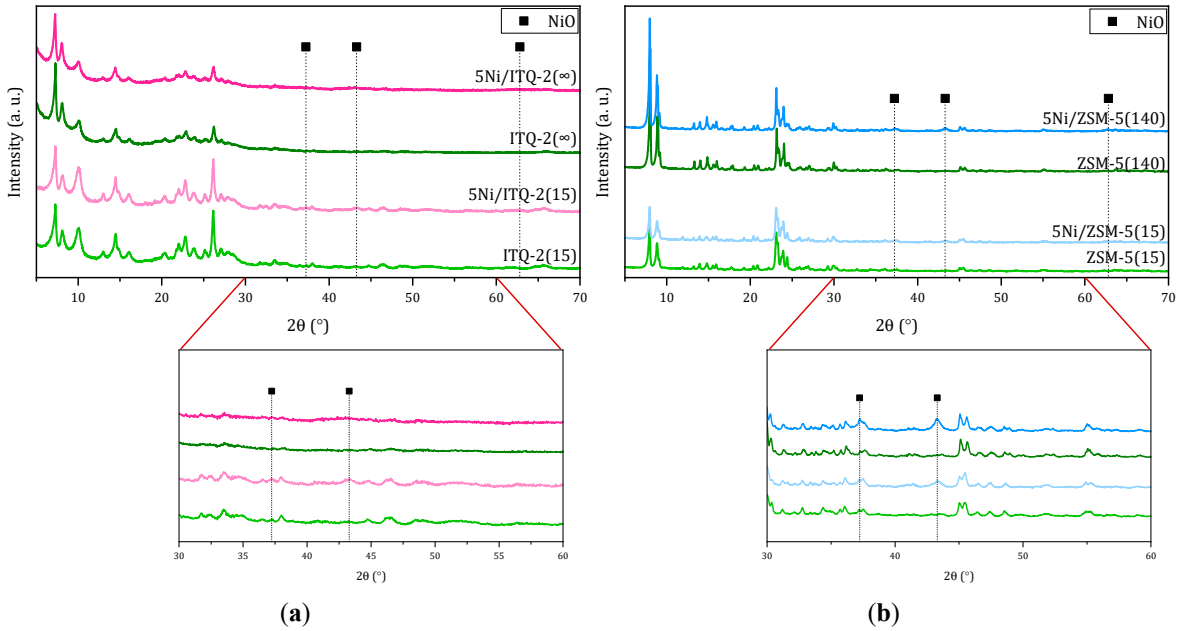


**Figure 1.** X-ray diffraction (XRD) patterns of the supports and the corresponding 5 wt.% Ni catalysts supported on (**a**) ITQ-2; (**b**) ZSM-5 with different Si/Al ratios.

In the case of ZSM-5 samples, NiO diffraction peaks are detected for both samples independently of the Si/Al ratio (Figure 1b). Crystallite sizes of 12.0 and 16.5 nm are obtained for 5Ni/ZSM-5(15) and 5Ni/ZSM-5(140), respectively. Therefore, the use of the delaminated zeolite ITQ-2 with a high Si/Al ratio seems to favor the formation of smaller NiO crystallite size.

Textural properties and chemical composition are summarized in Table 1. First of all, comparing ITQ-2 and ZSM-5 samples, the higher values of external surface area for the former group clearly stand out. Secondly, concerning the effects of Ni incorporation, a decrease of $S_{BET}$ was observed for all the samples. This fact is explained mainly by the dilution effect that takes place with Ni incorporation to the zeolite [30,31]. The variations of both external and micropore surface area were calculated to identify additional reasons. As the obtained values are higher than the expected values taking into account just the dilution effect, other reasons for the decrease of $S_{BET}$, such as the blockage of micropores, might also exist.

**Table 1.** Textural properties and chemical composition of the supports and the corresponding 5 wt.% Ni catalysts supported on ITQ-2 and ZSM-5 with different Si/Al ratios.

| Sample | Si/Al Ratio [1] | Ni Content [1] (wt.%) | $S_{BET}$ ($m^2/g$) | $S_{external}$ ($m^2/g$) | $S_{micropore}$ ($m^2/g$) |
|---|---|---|---|---|---|
| ITQ-2(∞) | | | 712 | 528 | 185 |
| 5Ni/ITQ-2(∞) | | 5.2 | 579 | 458 (−13%) | 120 (−35%) |
| ITQ-2(15) | 10 | | 610 | 284 | 325 |
| 5Ni/ITQ-2(15) | 10 | 5.7 | 520 | 213 (−25%) | 307 (−6%) |
| ZSM-5(140) | 117 | | 394 | 43 | 351 |
| 5Ni/ZSM-5(140) | 117 | 5.7 | 368 | 37 (−14%) | 331 (−6%) |
| ZSM-5(15) | 14 | | 429 | 40 | 389 |
| 5Ni/ZSM-5(15) | 15 | 5.3 | 373 | 40 (0%) | 333 (−14%) |

[1] Determined by ICP-OES.

Examining more carefully these calculated percentages, it can also be observed that for ZSM-5 samples, the variation of external and micropore surface areas follow opposite trends with Si/Al ratio. When the Si/Al ratio is increased, the variation of micropore surface area decreased up to the expected

value considering the dilution effect. However, the percentage of variation of external surface area increased suggesting that Ni nanoparticles are deposited in the external surface of this material. Metal can migrate during calcination to more internal positions providing greater stabilization. The acidic sites in the zeolites, which are more relevant in structures with a low Si/Al ratio, may act as anchoring sites for the migrated species [32,33]. In this way, the higher reduction of micropore surface area for ZSM-5(15) might be explained.

Regarding ITQ-2 samples, the two raw zeolites present considerable differences in the $S_{BET}$ values and, especially, in external surface area. These results indicate that the delamination is greater for ITQ-2(∞), being coherent with the fact that a decreasing Al content favors the delamination process [34].

$H_2$-TPR was performed to study the reduction behavior of the supported NiO particles. The results show that the incorporated Ni is reduced in the range 200−550 °C (Figure 2). In the case of the catalysts supported on ITQ-2, the profiles seem to be formed by broader components suggesting a greater heterogeneity regarding size of NiO nanoparticles and interaction with the support. Ni in the form of NiO located in the external surface of the zeolite is reported to be reduced between 330 and 385 °C [15,20], while Ni interacting in a higher degree with ITQ-2 can be reduced at 400 °C [35]. As it can be seen, the component at higher temperatures dominates the profiles of these samples. This finding supports that a higher Ni dispersion is obtained when it is dispersed on delaminated ITQ-2, as it was already indicated by XRD results. Nevertheless, the larger level of reducibility of the nickel catalyst supported on ITQ-2 (15) compared to the pure silica ITQ-2 (41% and 54%, respectively) seems to indicate that the nickel interaction with the support would be slightly higher for the pure silica ITQ-2 zeolite, explaining the lower size of the NiO nanoparticles detected in this sample.

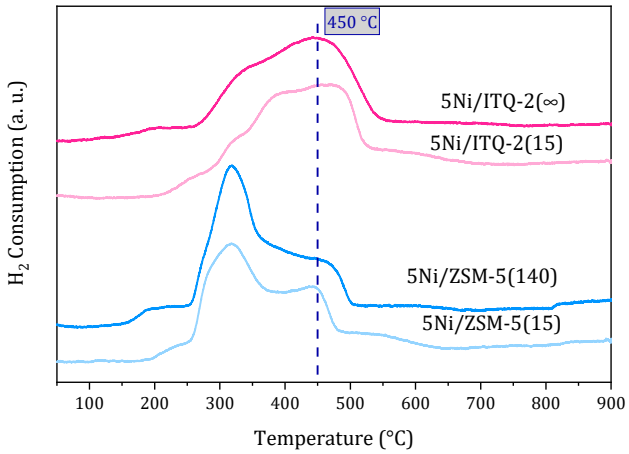


**Figure 2.** $H_2$-TPR profiles of the 5 wt.% Ni catalysts supported on ITQ-2 and ZSM-5 with different Si/Al ratios.

For the catalysts supported on ZSM-5, Ni reduction takes place within a similar range of temperatures. However, for these samples, the contribution at lower temperatures is predominant. This peak has been attributed to the reduction of bulk NiO, while the one at higher temperatures is related to smaller NiO nanoparticles or NiO inside the zeolite pores [36,37].

To evaluate the Brønsted acidity of these samples, pyridine adsorption at different temperatures was followed by FTIR. The amount of adsorbed pyridine in the catalyst was calculated from the area of the band at 1545 $cm^{-1}$, which is assigned to Brønsted acidity [28]. The results can be seen in Table 2. These tests revealed that the sample supported on pure silica ITQ-2 shows no Brønsted acidity, as expected due to the absence of Al in this material. Its counterpart (ITQ-2(15)) presents a slightly higher acid character. ZSM-5 samples follow a similar trend, that is, the sample with higher Al content shows a higher Brønsted acidity. However, in this case the difference was broader than in the case of ITQ-2 samples. The increase of Brønsted acidity with Al content is in good agreement with previous results [38,39].

**Table 2.** Brønsted acidity of the 5 wt.% Ni catalysts supported on ITQ-2 and ZSM-5 with different Si/Al ratios.

| Sample | Brønsted Acidity (mmol Pyridine/$g_{cat}$) | | |
|---|---|---|---|
| | **150 °C** | **250 °C** | **350 °C** |
| 5Ni/ITQ-2(∞) | 0.000 | 0.000 | 0.000 |
| 5Ni/ITQ-2(15) | 0.072 | 0.026 | 0.000 |
| 5Ni/ZSM-5(140) | 0.059 | 0.047 | 0.037 |
| 5Ni/ZSM-5(15) | 0.260 | 0.240 | 0.177 |

In previous studies, it is pointed out that Brønsted acidity is related to the hydrophobicity of the material. In general, for a given zeolite type, materials with lower Brønsted acidity also presents a higher hydrophobic character [40,41]. This hydrophobicity character might be relevant in this particular reaction, as water is one of the reaction products.

HR-TEM was performed to examine $Ni^0$ particle sizes in the reduced catalysts (Figure 3). A narrow particle size distribution was obtained for the catalyst 5Ni/ITQ-2(∞) with a very small mean particle size (2.4 nm). The rest of the samples show a wider particle size distribution with bigger $Ni^0$ particles, especially for ZSM-5 supported catalysts for which sizes between 5 and 40 nm were found.

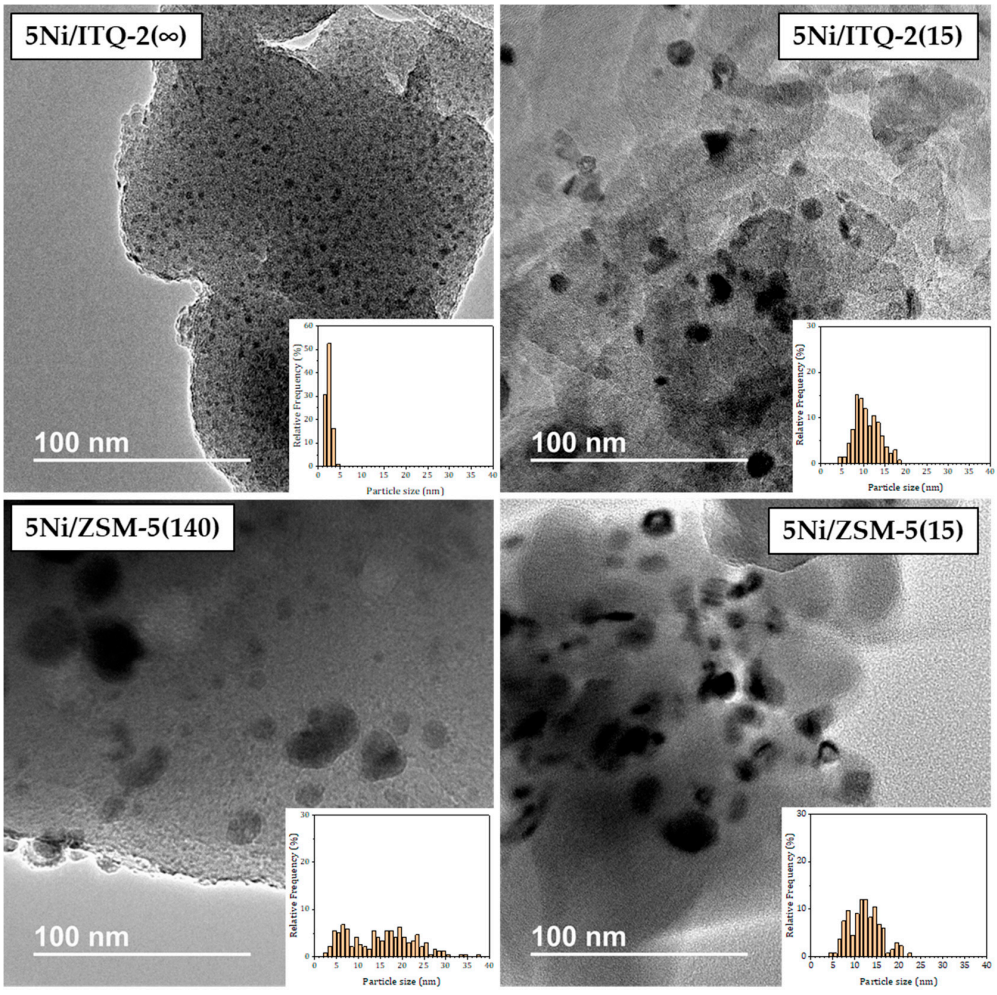


**Figure 3.** HR-TEM images and $Ni^0$ particle size distribution of the 5 wt.% Ni catalyst supported on ITQ-2 and ZSM-5 with different Si/Al ratios. Images correspond to reduced fresh catalyst before the methanation reaction.

### 3.2. Catalytic Activity

The catalytic activity of the prepared zeolite-supported Ni catalysts in the $CO_2$ methanation reaction was evaluated in a fixed-bed reactor. The $CO_2$ conversion and $CH_4$ selectivity obtained with these samples are presented in Figure 4 as a function of temperature. $CO_2$ conversion was found to increase with temperature as expected (Figure 4a). Generally, the more active catalysts also showed higher selectivity to $CH_4$ being the only by-product CO (Figure 4b).

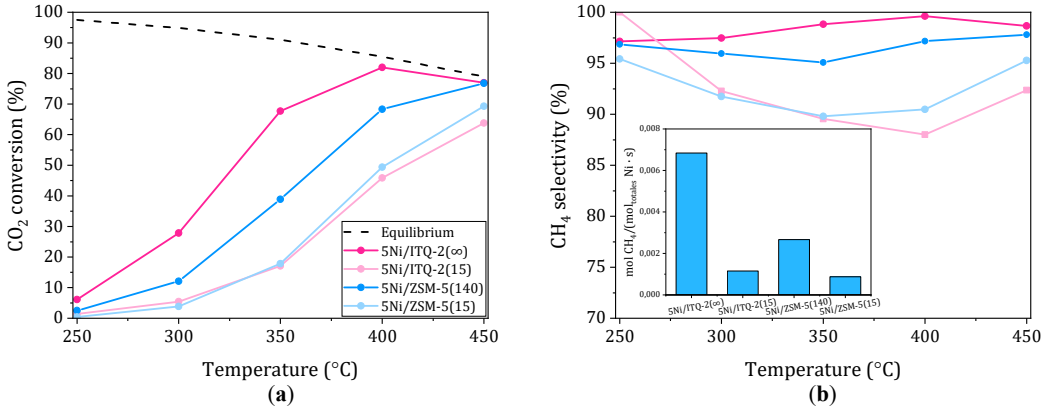


**Figure 4.** (**a**) $CO_2$ conversion; (**b**) $CH_4$ selectivity; (inset) reaction rate at 300 °C of the 5 wt.% Ni catalysts supported on ITQ-2 and ZSM-5 with different Si/Al ratios. Equilibrium values [8].

Attending to the ITQ-2 samples, a higher $CO_2$ conversion was obtained with the catalyst supported on the ITQ-2 without Al. Indeed, only with these catalyst equilibrium values were reached at 400 °C. The difference between the two samples supported on ITQ-2 was a maximum at 350 °C reaching 50 points. The higher catalytic performance of the catalyst supported on the pure silica ITQ-2 can be mainly attributed to the enhanced Ni dispersion in this sample related to the larger external surface area of the support. Furthermore, the absence of Brønsted acidity of this sample can be related to a strong hydrophobic character [40,41] favoring, hence, the removal of water from active sites and the reaction according to Chatelier's principle. The positive effect of the removal of water for the $CO_2$ methanation reaction has been reported previously [24,25,42].

Regarding the catalytic results of the catalysts supported on ZSM-5, a similar trend was observed. In this case, a minor difference was appreciated, but still, the ZSM-5 with a higher Si/Al ratio shows a $CO_2$ conversion 20 points greater than its counterpart. These two samples supported on ZSM-5 present similar NiO particle sizes, textural properties and reducibility. However, the sample supported on the ZSM-5 with a higher Si/Al ratio shows a distinctly lower Brønsted acidity suggesting that this sample is probably more hydrophobic [40,41]. This is coherent with previous studies, which reported that the increase of the Si/Al ratio of the ZSM-5 zeolite leads to a more hydrophobic material [43]. Furthermore, the $N_2$ adsorption results seem to indicate that Ni is preferentially deposited in the external surface area in the sample with a higher Si/Al ratio. Thus, the accessibility of the reactants to the active sites would be enhanced and the catalytic activity improved.

The catalysts used in these tests were characterized after the reaction. Carbon deposition was not detected for any of the catalysts here studied, suggesting that deactivation by coke disposition is not occurring, at least in the reaction time here considered (15 h). Furthermore, XRD patterns corroborate that both zeolite structures are well preserved (Figure 5). On the other hand, concerning Ni diffraction peaks, no peaks corresponding to NiO can be distinguished. Instead, diffraction peaks of reduced Ni ($Ni^0$) can be clearly seen only in the case of ZSM-5. This again supports the fact that a better distribution of Ni with a smaller crystallite size is obtained using the delaminated zeolite ITQ-2. HR-TEM images confirm that $Ni^0$ particles seem to suffer a very slight sinterization during the reaction. Nevertheless,

$Ni^0$ particle size distribution for the sample 5Ni/ITQ-2(∞) is still narrow and very similar to the size before reaction (2.8 nm after reaction against 2.4 nm before reaction) (Figure 6).

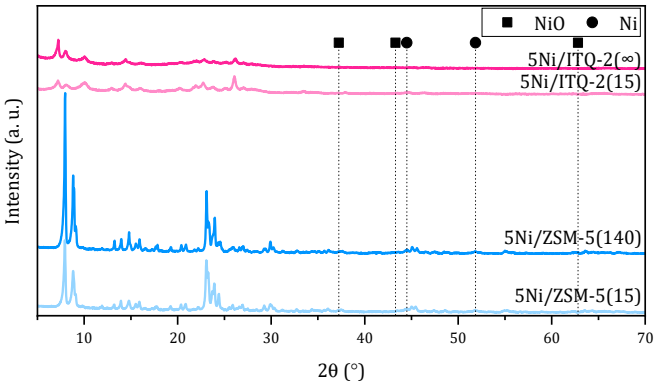


**Figure 5.** XRD patterns of the 5 wt.% Ni catalysts supported on ITQ-2 and ZSM-5 with different Si/Al ratios after the reaction test.

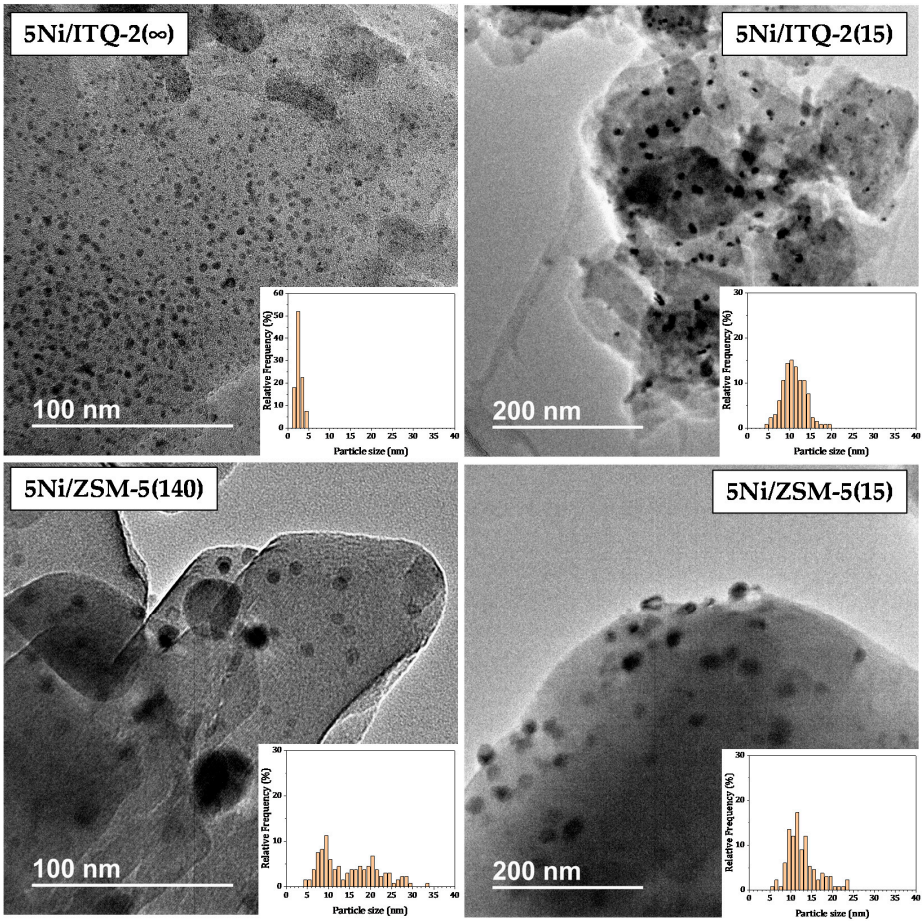


**Figure 6.** High-resolution transmission electron microscopy (HR-TEM) images and $Ni^0$ particle size distribution of the 5 wt.% Ni catalyst supported on ITQ-2 and ZSM-5 with different Si/Al ratios. Images obtained after the methanation reaction.

Comparing the catalytic results for both types of framework (ITQ-2 and ZSM-5), the performance is different depending on the Al content of the support. With the support of high Al content, a similar catalytic behavior was obtained, independently of the type of zeolite. However, the decrease in Al content of the support leads to a markedly enhanced catalytic activity of the delaminated ITQ-2,

which is probably related to the small NiO crystallite size found for this sample by XRD. The catalyst supported on pure silica ITQ-2 was the one which allows obtaining a higher $CO_2$ conversion and $CH_4$ selectivity. This leads to a distinctly greater reaction rate for the sample 5Ni/ITQ-2(∞) with values at least 150% higher than those of the rest of the samples of this study (Figure 4b inset). The similar performance of the materials with higher Al content (lower Si/Al ratio) might be explained for the similar crystallite size of NiO in these two samples (10.6 and 12.0 nm for the ITQ-2(15) and ZSM-5(15) supported catalysts, respectively). In addition, the Si/Al ratio of the ITQ-2(15) was found to be lower than the expected value, which is probably detrimental for its activity.

These results suggest that the Al content of the zeolite has a more relevant effect than the zeolite type in the properties of the final catalyst. Si/Al ratio is reported to have influence in Brønsted acidity and, thus, in hydrophobicity for a given zeolite type [38–41]. In this way, more hydrophobic materials would remove water from active sites more efficiently, favoring the development of the reaction [24,25,42]. The Si/Al ratio might also affect the dispersion and stability of Ni nanoparticles. Rosetti et al. [44] claimed that for Ni supported on Beta zeolite, a high Si/Al ratio favored both an initial dispersion of Ni and the redispersion with subsequent thermal treatments.

The results obtained in our study show that for both zeolite types (ITQ-2 and ZSM-5), the higher the Si/Al ratio, the better catalytic activity, which is in accordance to the reported results for Ni catalysts supported on zeolite Y [25] and Beta [24]. Among the catalysts considered, the catalyst supported on the pure silica ITQ-2 allow to obtain the highest yield to $CH_4$. In Table 3, its activity is compared with the values reported for other similar catalysts. First, it is important to mention that a delaminated zeolite is considered as support for $CO_2$ methanation for the first time in this reaction. This is noteworthy as, according to previous studies, zeolite type has an influence on the final activity of the material [15,20,24] and delaminated zeolites present unique and particular features worth studying for this reaction. Intrinsic properties of each zeolite type, such as its pores system, pore sizes or hydrophobicity, are reported to affect Ni dispersion and, thus, catalytic activity.

In particular, ITQ-2 presents a large external surface area, which allows obtaining a very small NiO crystallite size in comparison with other studies. The decrease in crystallite sizes of Ni species has been achieved in previous studies with the use of support with high surface area, such as MSN [17], different precursor [20] or by addition of promoters [15,21,22]. For example, a decrease for $Ni^0$ from 20.1 to 8.7 nm was achieved by the addition of $La_2O_3$ [15] and from 19.4 to 2.4 nm with Ce incorporation [22]. This decrease in $Ni^0$ crystallite size resulted in an improved catalytic activity, evidencing that Ni particle size is one of the key factors for the successful development of methanation reaction.

The comparison of the results of catalytic activity of different studies is not straightforward as the experimental conditions differ. GHSV, temperature and Ni content strongly affect the catalytic activity obtained. As an attempt to normalize the results to Ni content, for the studies with available data, a parameter "x" has been calculated from the ratio between $CO_2$ conversion and quantity of supported Ni. In general, it can be said that a lower GHSV is used in our study compared with previous works. However, the comparison of our data with the studies [20] and [45] is possible as the reaction conditions seem to be similar. First, it is important to remark that our value of GHSV (9000 mL/($g_{cat}$·h)) refers to the total flow of reactants ($CO_2$, $H_2$). On the contrary, the GHSV of study [20] is calculated from the total flow ($CO_2$, $H_2$, $N_2$), being the comparable value based on $CO_2$ and $H_2$ flows 3333 mL/($g_{cat}$·h). Taking this into account, it can be said that values for $CO_2$ conversion comparable with those of [20] and [45] are obtained with 5Ni/ITQ-2(∞). Moreover, a distinctly higher $CH_4$ selectivity is achieved, even though a slightly disadvantageous GHSV and lower Ni content are used in our study. Finally, attending to studies performed at higher GHSV, 5Ni/ITQ-2(∞) is far from the sample 5Ni/MSN [17] in terms of activity, being the later around twice more active operating at five times higher GHSV. On the other hand, it is also important to highlight that with 5Ni/ITQ-2(∞), similar values of $CH_4$ yield to those reported using promoted catalysts with $La_2O_3$ [15] or Ce [22] are achieved at 350 °C. It is true that the lower GHSV used in our study favor a higher catalytic performance, but also the Ni loading in our samples is only 5 wt.%.

**Table 3.** Comparison of the catalytic results obtained using a 5Ni/ITQ-2(∞) catalyst with those reported in the literature.

| Sample[1] | NiO Size (nm) | $Ni^0$ Size (nm) | GHSV | Temperature (°C) | $CO_2$ Conversion (%) | $CH_4$ Selectivity (%) | $x^2$ | Ref. |
|---|---|---|---|---|---|---|---|---|
| 5Ni/ITQ-2(∞) | <3 | | 9000 mL/($g_{cat}$·h) 3500 $h^{-1}$ | 250 | 6 | 97 | 154 | This work |
| | | | | 300 | 28 | 97 | 718 | |
| | | | | 350 | 68 | 99 | 1744 | |
| | | | | 400 | 82 | 99 | 2103 | |
| 5Ni13X-Cit | | | 13,333 mL/($g_{cat}$·h) | 240 | 17 | 71 | 378 | [20] |
| 10Ni/ZSM-5 | 14.3 | | 2000 $h^{-1}$ | 400 | 76 | ≈75 | | [45] |
| 10Ni/Na-BETA | | 20.1 | 10,000 $h^{-1}$ | 350 | 33 | 88 | 660 | [15] |
| 10Ni-10$La_2O_3$/Na-BETA | | 8.7 | 10,000 $h^{-1}$ | 350 | 65 | 99 | 1300 | [15] |
| 14Ni7Ce/USY | | | 15,000 $h^{-1}$ | 400 | 77 | 99 | 1023 | [23] |
| 14Ni7Ce/USY | | | 43,000 $h^{-1}$ | 400 | 68 | 95 | 2600 | [23] |
| 15Ni/Na-USY | 18 | 25 | 43,000 $h^{-1}$ | 350 | 55 | 95 | | [24] |
| 15Ni/Na-BEA | 16 | 18 | 43,000 $h^{-1}$ | 350 | 43 | 92 | | [24] |
| 15Ni/Na-ZSM-5 | 21 | 24 | 43,000 $h^{-1}$ | 350 | 40 | 85 | | [24] |
| 15Ni/Na-MOR | 26 | 23 | 43,000 $h^{-1}$ | 350 | 40 | 87 | | [24] |
| 15Ni-20Ce/Cs-USY | | | 43,000 $h^{-1}$ | 350 | ≈70 | ≈98 | | [22] |
| 5Ni/Na-USY | | 19.4 | 43,000 $h^{-1}$ | 400 | ≈20 | ≈60 | | [22] |
| 5Ni/3Ce/Na-USY | | 13.3 | 43,000 $h^{-1}$ | 400 | ≈34 | ≈70 | | [22] |
| 3Ce/5Ni/Na-USY | | 2.5 | 43,000 $h^{-1}$ | 400 | ≈38 | ≈75 | | [22] |
| 5Ni-3Ce/Na-USY | | 2.4 | 43,000 $h^{-1}$ | 400 | ≈40 | ≈80 | | [22] |
| 9Mg 13Ni/USY | | | 43,000 $h^{-1}$ | 400 | ≈60 | ≈95 | | [21] |
| 5Ni/MSN | 9.9 | | 50,000 mL/($g_{cat}$·h) | 300 | 64 | | 6400 | [17] |

[1] 5Ni13X-Cit = prepared using nickel citrate; 15Ni/Na-USY = supported on ultrastable zeolite Y; MSN = mesostructured silica nanoparticles. [2] x, calculated as the ratio between $CO_2$ conversion and Ni quantity in the reactor in grams, calculated from the mass of catalyst in the reactor and Ni loading.

## 4. Conclusions

In this work, the use of the delaminated zeolite ITQ-2 with high external surface area was considered for the first time in the synthesis of Ni-based catalysts for $CO_2$ methanation. Specifically, two samples with different Al content were investigated and compared with ZSM-5 materials of similar Si/Al ratios. For both types of zeolites, the increase of the Si/Al ratio results in an improvement of the catalytic activity of the material. This fact can be explained by the higher hydrophobicity of the materials with a higher Si/Al ratio, which can be inferred from their lower Brønsted acidity. Comparing both structures, a similar performance is obtained for the catalysts supported on zeolite with a Si/Al ratio of 15. However, a distinctly higher performance is achieved with 5Ni/ITQ-2(∞). In particular, for the catalyst supported on pure silica ITQ-2, NiO diffraction peaks were not detected, indicating a smaller crystallite size in this sample. By HR-TEM, it is confirmed that Ni is well dispersed in this sample after reduction and reaction with a narrow particle size distribution and a mean particle size around 2.5 nm. This fact is probably related to the larger external surface area of its support. These results explain its superior catalytic activity. With this catalyst, a $CO_2$ conversion of 68% with a $CH_4$ selectivity higher than 98% was obtained at 350 °C, which means an improvement of 50 points in $CO_2$ conversion when compared with the catalyst supported on ITQ-2 with lower Si/Al ratio. The results here obtained with 5Ni/ITQ-2(∞) are comparable to those presented in other studies using zeolite-supported Ni catalysts with promoters such as $La_2O_3$ or Ce.

**Author Contributions:** Conceptualization, C.C.-M. and A.C.; methodology, C.C.-M; investigation, C.C.-M., J.F.D.C.-S. and A.C.; writing—original draft preparation, C.C.-M.; writing—review and editing, C.C.-M., A.C. and J.F.D.C.-S.; supervision, A.C.; project administration, A.C.; funding acquisition, A.C. All authors have read and agreed to the published version of the manuscript.

**Funding:** This research was funded by the Spanish Ministry of Science, Innovation and Universities, grant numbers SVP-2014-068713 and RTI2018-102161-B-I00.

**Acknowledgments:** The authors thank Urbano Díaz for supplying the samples of ITQ-2 zeolite.

**Conflicts of Interest:** The authors declare no conflict of interest.

## References

1. IPCC: Climate Change 2014: Synthesis Report. Contribution of Working Groups I, II and III to the Fifth Assessment Report of the Intergovernmental Panel on Climate Change. Available online: https://www.ipcc.ch/report/ar5/syr/ (accessed on 26 May 2020).
2. Le Quéré, C.; Jackson, R.B.; Jones, M.W.; Smith, A.J.P.; Abernethy, S.; Andrew, R.M.; De-Gol, A.J.; Willis, D.R.; Shan, Y.; Canadell, J.G.; et al. Temporary reduction in daily global $CO_2$ emissions during the COVID-19 forced confinement. *Nat. Clim. Chang.* **2020**, *19*, 1–7.
3. Muhammad, S.; Long, X.; Salman, M. COVID-19 pandemic and environmental pollution: A blessing in disguise? *Sci. Total Environ.* **2020**, *728*, 138820. [CrossRef] [PubMed]
4. Zambrano-Monserrate, M.A.; Ruano, M.A.; Sanchez-Alcalde, L. Indirect effects of COVID-19 on the environment. *Sci. Total Environ.* **2020**, *728*, 138813. [CrossRef] [PubMed]
5. United Nations Framework Convention on Climate Change: The Paris Agreement. Available online: https://unfccc.int/process-and-meetings/the-paris-agreement/the-paris-agreement (accessed on 26 May 2020).
6. IPCC: Global Warming of 1.5 °C. An IPCC Special Report on the Impacts of Global Warming of 1.5 °C above Pre-Industrial Levels and Related Global Greenhouse Gas Emission Pathways, in the Context of Strengthening the Global Response to the Threat of Climate Change, Sustainable Development, and Efforts to Eradicate Poverty. Available online: https://www.ipcc.ch/sr15/download/#full (accessed on 26 May 2020).
7. Gao, J.; Wang, Y.; Ping, Y.; Hu, D.; Xu, G.; Gu, F.; Su, F. A thermodynamic analysis of methanation reactions of carbon oxides for the production of synthetic natural gas. *RSC Adv.* **2012**, *2*, 2358–2368. [CrossRef]
8. Sahebdelfar, S.; Takht Ravanchi, M. Carbon dioxide utilization for methane production: A thermodynamic analysis. *J. Petrol. Sci. Eng.* **2015**, *134*, 14–22. [CrossRef]
9. Aziz, M.A.A.; Jalil, A.A.; Triwahyono, S.; Ahmad, A. $CO_2$ methanation over heterogeneous catalysts: Recent progress and future prospects. *Green Chem.* **2015**, *17*, 2647–2663. [CrossRef]

10. Frontera, P.; Macario, A.; Ferraro, M.; Antonucci, P. Supported catalysts for $CO_2$ methanation: A review. *Catalysts* **2017**, *7*, 59. [CrossRef]
11. Recent trend in thermal catalytic low temperature CO2 methanation: A critical review. Available online: https://doi.org/10.1016/j.cattod.2020.02.017 (accessed on 24 July 2020).
12. Younas, M.; Loong Kong, L.; Bashir, M.J.K.; Nadeem, H.; Shehzad, A.; Sethupathi, S. Recent Advancements, Fundamental Challenges, and Opportunities in Catalytic Methanation of $CO_2$. *Energy & Fuels* **2016**, *30*, 8815–8831.
13. Lu, X.; Gu, F.; Liu, Q.; Gao, J.; Liu, Y.; Li, H.; Jia, L.; Xu, G.; Zhong, Z.; Su, F. VOx promoted Ni catalysts supported on the modified bentonite for CO and $CO_2$ methanation. *Fuel Process. Technol.* **2015**, *135*, 34–46. [CrossRef]
14. Guilera, J.; del Valle, J.; Alarcón, A.; Díaz, J.A.; Andreu, T. Metal-oxide promoted Ni/Al2O3 as CO2 methanation micro-size catalysts. *J. CO2 Util.* **2019**, *30*, 11–17. [CrossRef]
15. Quindimil, A.; De-La-Torre, U.; Pereda-Ayo, B.; González-Marcos, J.A.; González-Velasco, J.R. Ni catalysts with La as promoter supported over Y- and BETA- zeolites for CO2 methanation. *Appl. Catal. B-Environ.* **2018**, *238*, 393–403. [CrossRef]
16. Le, T.A.; Kim, M.S.; Lee, S.H.; Kim, T.W.; Park, E.D. CO and CO2 methanation over supported Ni catalysts. *Catal. Today* **2017**, *293–294*, 89–96. [CrossRef]
17. Aziz, M.A.A.; Jalil, A.A.; Triwahyono, S.; Mukti, R.R.; Taufiq-Yap, Y.H.; Sazegar, M.R. Highly active Ni-promoted mesostructured silica nanoparticles for CO2 methanation. *Appl. Catal. B-Environ.* **2014**, *147*, 359–368. [CrossRef]
18. Bacariza, M.C.; Graça, I.; Lopes, J.M.; Henriques, C. Tuning zeolite properties towards CO2 methanation: An overview. *ChemCatChem* **2019**, *11*, 2388–2400. [CrossRef]
19. Bacariza, M.C.; Graça, I.; Westermann, A.; Ribeiro, M.F.; Lopes, J.M.; Henriques, C. CO2 Hydrogenation Over Ni-Based Zeolites: Effect of Catalysts Preparation and Pre-reduction Conditions on Methanation Performance. *Top. Catal.* **2016**, *59*, 314–325. [CrossRef]
20. Influence of nickel precursors on the properties and performance of Ni impregnated zeolite 5A and 13X catalysts in CO2 methanation. Available online: https://doi.org/10.1016/j.cattod.2020.05.025 (accessed on 24 July 2020).
21. Bacariza, M.C.; Graça, I.; Bebiano, S.S.; Lopes, J.M.; Henriques, C. Magnesium as Promoter of CO2 Methanation on Ni-Based USY Zeolites. *Energy & Fuels* **2017**, *31*, 9776–9789.
22. Bacariza, M.C.; Graça, I.; Lopes, J.M.; Henriques, C. Ni-Ce/Zeolites for CO2 Hydrogenation to CH4: Effect of the Metal Incorporation Order. *ChemCatChem* **2018**, *10*, 2773–2781. [CrossRef]
23. Graça, I.; González, L.V.; Bacariza, M.C.; Fernandes, A.; Henriques, C.; Lopes, J.M.; Ribeiro, M.F. CO2 hydrogenation into CH4 on NiHNaUSY zeolites. *Appl. Catal. B-Environ.* **2014**, *147*, 101–110. [CrossRef]
24. Bacariza, M.C.; Maleval, M.; Graça, I.; Lopes, J.M.; Henriques, C. Power-to-methane over Ni/zeolites: Influence of the framework type. *Microporous Mesoporous Mater.* **2019**, *274*, 102–112. [CrossRef]
25. Bacariza, M.C.; Graça, I.; Lopes, J.M.; Henriques, C. Enhanced activity of CO2 hydrogenation to CH4 over Ni based zeolites through the optimization of the Si/Al ratio. *Microporous Mesoporous Mater.* **2018**, *267*, 9–19. [CrossRef]
26. Bacariza, M.C.; Bértolo, R.; Graça, I.; Lopes, J.M.; Henriques, C. The effect of the compensating cation on the catalytic performances of Ni/USY zeolites towards $CO_2$ methanation. *J. CO2 Util.* **2017**, *21*, 280–291. [CrossRef]
27. Nicolopoulos, S.; González-Calbet, J.M.; Vallet-Regi, M.; Camblor, M.A.; Corell, C.; Corma, A.; Diaz-Cabañas, M.J. Use of Electron Microscopy and Microdiffraction for Zeolite Framework Comparison. *J. Am. Chem. Soc.* **1997**, *119*, 11000–11005. [CrossRef]
28. Emeis, C.A. Determination of Integrated Molar Extinction Coefficients for Infrared Absorption Bands of Pyridine Adsorbed on Solid Acid Catalysts. *J. Catal.* **1993**, *141*, 347–354. [CrossRef]
29. Uvarov, V.; Popov, I. Metrological characterization of X-ray diffraction methods for determination of crystallite size in nano-scale materials. *Mater. Charact.* **2007**, *58*, 883–891. [CrossRef]
30. Concepción, P.; López, C.; Martínez, A.; Puntes, V.F. Characterization and catalytic properties of cobalt supported on delaminated ITQ-6 and ITQ-2 zeolites for the Fischer—Tropsch synthesis reaction. *J. Catal.* **2004**, *228*, 321–332. [CrossRef]

31. Da Costa-Serra, J.F.; Navarro, M.T.; Rey, F.; Chica, A. Bioethanol steam reforming on Ni-based modified mordenite. Effect of mesoporosity, acid sites and alkaline metals. *Int. J. Hydrog. Energy* **2012**, *37*, 7101–7108. [CrossRef]
32. Mariscal, R.; Navarro, R.M.; Pawelec, B.; Fierro, J.L.G. Factors affecting Ni-sulfide formation in Y-type zeolites: A combined Fourier transform infrared and X-ray photoelectron spectroscopy study. *Microporous Mesoporous Mater.* **2000**, *34*, 181–194. [CrossRef]
33. Romero, M.D.; Calles, J.A.; Rodríguez, A.; Cabanelas, J.C. The Influence of Calcination Treatment over Bifunctional Ni/HZSM-5 Catalysts. *Ind. Eng. Chem. Res.* **1998**, *37*, 3846–3852. [CrossRef]
34. Frontera, P.; Testa, F.; Aiello, R.; Candamano, S.; Nagy, J.B. Transformation of MCM-22(P) into ITQ-2: The role of framework aluminium. *Microporous Mesoporous Mater.* **2007**, *106*, 107–114. [CrossRef]
35. Chica, A.; Sayas, S. Effective and stable bioethanol steam reforming catalyst based on Ni and Co supported on all-silica delaminated ITQ-2 zeolite. *Catal. Today* **2009**, *146*, 37–43. [CrossRef]
36. Maia, A.J.; Louis, B.; Lam, Y.L.; Pereira, M.M. Ni-ZSM-5 catalysts: Detailed characterization of metal sites for proper catalyst design. *J. Catal.* **2010**, *269*, 103–109. [CrossRef]
37. Mohan, V.; Raghavendra, C.; Pramod, C.V.; Raju, B.D.; Rama Rao, K.S. Ni/H-ZSM-5 as a promising catalyst for vapour phase hydrogenation of levulinic acid at atmospheric pressure. *RSC Adv.* **2014**, *4*, 9660–9668. [CrossRef]
38. Martínez, A.; Peris, E.; Sastre, G. Dehydroaromatization of methane under non-oxidative conditions over bifunctional Mo/ITQ-2 catalysts. *Catal. Today* **2005**, *107–108*, 676–684. [CrossRef]
39. Semelsberger, T.A.; Ott, K.C.; Borup, R.L.; Greene, H.L. Role of acidity on the hydrolysis of dimethyl ether (DME) to methanol. *Appl. Catal. B-Environ.* **2005**, *61*, 281–287. [CrossRef]
40. Yonli, A.H.; Batonneau-Gener, I.; Koulidiati, J. Adsorptive removal of α-endosulfan from water by hydrophobic zeolites. An isothermal study. *J. Hazard. Mater.* **2012**, *203–204*, 357–362. [CrossRef] [PubMed]
41. Yonli, A.H.; Gener, I.; Mignard, S. Comparative study of the hydrophobicity of BEA, HZSM-5 and HY zeolites determined by competitive adsorption. *Microporous Mesoporous Mater.* **2010**, *132*, 37–42. [CrossRef]
42. Borgschulte, A.; Gallandat, N.; Probst, B.; Suter, R.; Callini, E.; Ferri, D.; Arroyo, Y.; Erni, R.; Geerlings, H.; Züttel, A. Sorption enhanced CO2 methanation. *Phys. Chem. Chem. Phys.* **2013**, *15*, 9620–9625. [CrossRef]
43. Changkhamchom, S.; Sirivat, A. High proton conductivity ZSM-5/sulfonated poly(ether ketone ether sulfone) (S-PEKES) composite proton exchange membrane for using in direct methanol fuel cell. *Solid State Ionics* **2014**, *263*, 161–166. [CrossRef]
44. Rossetti, I.; Compagnoni, M.; Finocchio, E.; Ramis, G.; Di Michele, A.; Zucchini, A.; Dzwigaj, S. Syngas production via steam reforming of bioethanol over Ni—BEA catalysts: A BTL strategy. *Int. J. Hydrog. Energy* **2016**, *41*, 16878–16889. [CrossRef]
45. Guo, X.; Traitangwong, A.; Hu, M.; Zuo, C.; Meeyoo, V.; Peng, Z.; Li, C. Carbon Dioxide Methanation over Nickel-Based Catalysts Supported on Various Mesoporous Material. *Energy & Fuels* **2018**, *32*, 3681–3689.